Off-Equatorial Pi2 Pulsations Inside and Outside the Plasmapause Observed by the Arase Satellite

著者	Teramoto M., Miyoshi Y., Matsuoka A., Kasahara Y., Kumamoto A., Tsuchiya F., Nose M., Imajo S., Shoji M., Nakamura S., Kitahara M., Shnohara I.
journal or publication title	Journal of Geophysical Research: Space Physics
volume	127
number	1
page range	e2021JA029677-1-e2021JA029677-18
year	2021-12-10
その他のタイトル	Off-equatorial Pi2 pulsations Inside and Outside the plasmapause observed by the Arase satellite
URL	http://hdl.handle.net/10228/00009054

doi: https://doi.org/10.1029/2021JA029677

JGR Space Physics

RESEARCH ARTICLE
10.1029/2021JA029677

Key Points:

- A statistical study of off-equatorial Pi2 pulsations was conducted using magnetic field and electron density data from the Arase satellite
- Most events that had high coherence with low-latitude ground Pi2 were dominated by the compressional component
- The cross-phase and power distributions of high-coherence events were consistent with the plasmaspheric virtual resonance mode

Supporting Information:

Supporting Information may be found in the online version of this article.

Correspondence to:

M. Teramoto,
teramoto.mariko418@mail.kyutech.jp

Citation:

Teramoto, M., Miyoshi, Y., Matsuoka, A., Kasahara, Y., Kumamoto, A., Tsuchiya, F., et al. (2022). Off-equatorial Pi2 pulsations inside and outside the plasmapause observed by the Arase satellite. *Journal of Geophysical Research: Space Physics*, *127*, e2021JA029677. https://doi.org/10.1029/2021JA029677

Received 19 JUN 2021
Accepted 30 NOV 2021

Author Contributions:

Data curation: A. Matsuoka, Y. Kasahara, A. Kumamoto, F. Tsuchiya, S. Imajo, M. Shoji, S. Nakamura, M. Kitahara
Project Administration: Y. Miyoshi, I. Shnohara
Resources: A. Matsuoka, Y. Kasahara, A. Kumamoto, F. Tsuchiya, M. Shoji
Software: S. Imajo, M. Shoji, S. Nakamura, M. Kitahara
Supervision: Y. Miyoshi, M. Nosé
Writing – review & editing: Y. Miyoshi, M. Nosé

Off-Equatorial Pi2 Pulsations Inside and Outside the Plasmapause Observed by the Arase Satellite

M. Teramoto[1], Y. Miyoshi[2], A. Matsuoka[3], Y. Kasahara[4], A. Kumamoto[5], F. Tsuchiya[5], M. Nosé[2], S. Imajo[3], M. Shoji[2], S. Nakamura[2], M. Kitahara[2], and I. Shnohara[6]

[1]Graduate School of Engineering, Kyushu Institute of Technology, Kitakusyu, Japan, [2]Institute for Space-Earth Environmental Research, Nagoya University, Nagoya, Japan, [3]Data Analysis Center for Geomagnetism and Space Magnetism, Graduate School of Science, Kyoto University, Kyoto, Japan, [4]Graduate School of Natural Science and Technology, Kanazawa University, Kanazawa, Japan, [5]Department of Geophysics, Graduate School of Science, Tohoku University, Sendai, Japan, [6]Institute of Space and Astronautical Science, Japan Aerospace Exploration Agency, Sagamihara, Japan

Abstract Using magnetic field and electron density data from the Arase satellite for the period from March 2017 to September 2019, we investigate the spatial properties of Pi2 pulsations in relation to the plasmapause over a wide latitudinal range (absolute magnetic latitude, |Mlat|, < 45°) in the inner magnetosphere. Magnetic field disturbances that have high coherence (> 0.7) with Pi2 pulsations in the north-south (H) component at low-latitude ground stations on the nightside, are dominantly identified from the magnetic fields in the radial (B_R) and compressional (B_P) components when the satellite is in the pre-midnight sector. In particular, high-coherence B_P events are distributed over wide L-values and latitudinal ranges on the nightside in the pre-midnight sector. We identify the location of the plasmapause using the electron densities measured by Arase, and found that the B_P-H power ratio and the cross phases of the high-coherence events show a gradual peak and a clear phase change from 0° to 180° in the vicinity of the plasmapause, respectively. These features indicate that mid- and low-latitude Pi2 pulsations on the nightside are excited by the plasmaspheric virtual resonance mode.

1. Introduction

Pi2 pulsations are irregular ultra low frequency waves in the geomagnetic field with a period of 40–150 s (Jacobs, 1970). They occur over a wide latitudinal range from low to high latitudes on the nightside during substorm expansions or pseudo-breakups. Mid- and low-latitude Pi2 pulsations are utilized as indicators of substorm onset (Keiling & Takahashi, 2011; Rostoker et al., 1980). Two excitation mechanisms have been proposed for the generation of mid- and low-latitude Pi2 pulsations: the plasmaspheric cavity (PC) mode resonance (Saito & Matsushita, 1968) and direct driving by periodic bursty bulk flows (BBFs) models (Kepko & Kivelson, 1999; Kepko et al., 2001).

PC mode resonance is excited by compressional waves with broadband frequencies that propagate earthward from the current disruption region in the equatorial plane at substorm onset. After the compressional waves reach the plasmasphere, their energy is trapped in the Alfven speed (V_A) well structure between the inner and outer boundaries (the ground or the ionosphere at low latitudes and the plasmapause, respectively), at which V_A is enhanced. The compressional waves are reflected back and forth between the boundaries, and radial standing waves are excited in the plasmasphere. The eigenfrequency of these PC mode waves depends on the mass density of the plasmasphere and the radial distance between the two boundaries in the equatorial plane. In PC mode resonance, the poloidal mode waves are dominant and have a common frequency in the plasmasphere (Takahashi et al., 1995). Because the plasmapause structure varies with geomagnetic activity and the radial profile of the V_A changes, the plasmapause is not always a perfect reflector. Lee (1996) suggested the plasmaspheric virtual resonance (PVR) mode, in which the energy of radial standing waves leaks from the plasmasphere owing to an imperfect plasmapause boundary. In the PVR mode, eigenmode waves are formed by a process similar to the PC mode in the plasmasphere. However, the poloidal mode waves exist both inside and outside the plasmasphere in the PVR mode, while the poloidal waves in the PC mode are confined to the plasmasphere.

The direct BBF-driven model represents a different school of thought. In this model, periodic earthward plasma flows directly drive mid- and low-latitude Pi2 pulsations (Kepko & Kivelson, 1999; Kepko et al., 2001). At substorm onset, the periodic plasma flows in the plasmasheet reach the boundary between the dipolar and tail-like fields and decelerate or brake (Angelopoulos et al., 1992). The braking of the periodic flow bursts generates compressional pulses that propagate earthward and directly excite Pi2 pulsations in the inner magnetosphere. In the direct BBF-driven model, each plasma pulse in the plasmasheet generates a pulse in the geomagnetic field. Therefore, the periodicities of the Pi2 pulsations in the inner magnetosphere are determined by the flow periodicities in the plasmasheet. Because the compressional waves excited by the periodic plasma flow propagate from the braking region to the near-earth region, Pi2 pulsations that are directly excited by periodic BBFs propagate radially; they also have a common frequency in the entire inner magnetosphere from the braking region to the inner magnetosphere.

To investigate the propagation mode and generation mechanism of mid- and low-latitude Pi2 pulsations, in-situ observations of the inner magnetosphere using satellites are important, because they provide data on the spatial characteristics of magnetic disturbances in the inner magnetosphere. Through a systematic statistical study using the equatorially orbiting Active Magnetospheric Particle Tracer Explorer (AMPTE) Charge Composition Explorer (CCE) magnetometer data, Takahashi et al. (1995) showed the spatial properties of Pi2 pulsations in the inner magnetosphere at $L < 7$ and $|\mathrm{Mlat}| < 16°$. They identified magnetic disturbances that had high coherence with Pi2 range pulsations at low-latitude ground stations, and found that these high-coherence events were dominated by the poloidal (radial and compressional) components in the magnetic field. High-coherence events are primarily observed at $L < 5$ on the nightside. Using magnetic and electric field and plasma density data from the Combined Release and Radiation Effects satellite, Takahashi, Lee, et al. (2003) investigated the radial mode structure of Pi2 pulsations in the electric and magnetic fields at $L < 7$ and $|\mathrm{Mlat}| < 13°$ in relation to the plasmapause. They found that high-coherence events in the poloidal component were excited in the plasmasphere or near the plasmapause. Such studies using equatorial orbiting satellites provide evidence for PC mode-type oscillations, which are confined to the plasmasphere.

Even off the magnetic equator, high-coherence Pi2 pulsations have been reported by Osaki et al., (1998), Keiling et al. (2001), Kim et al. (2005), and Teramoto et al. (2008, 2011) using polar-orbiting satellites. Osaki et al. (1998) observed Pi2 pulsations off the equator (24°–40° Mlat) in the plasmasphere on the nightside for the first time, using the Akebono satellite. They reported two transverse Pi2 events, the Poynting fluxes of which indicate propagating features from the magnetic equator to the ionosphere along the magnetic field lines, rather than field-aligned standing features. As such, they concluded that the cavity model was not a suitable model to explain the off-equatorial Pi2 pulsations observed by Akebono. Using the magnetic and electric field data observed at 10°–14° Mlat, $L \sim 3.7$–4.1, and ∼23 magnetic local time (MLT) by the Polar satellite, Keiling et al. (2001) reported a toroidal mode Pi2 event with the standing wave properties of the field line resonance (FLR) coupled with the radially propagating fast mode waves. They also reported that the transverse Pi2 pulsations correlated well with Pi2 pulsations at mid- and low-latitude ground stations ($L < 4$) at 21–23 MLT. Kim et al. (2005) showed that 14 high-coherence events in the compressional component could be observed outside the plasmasphere off the equator (> 15°), identifying the location of the plasmapause from the electron number density inferred using the Polar satellite. High-coherence events have out-of-phase relationships to the Pi2 pulsations in the H component on the ground at low latitudes. Using the magnetic field data of the Dynamic Explorer (DE)-1 satellite and geomagnetic field data from low-latitude ground stations, Teramoto et al. (2008) showed the latitudinal profile of magnetic disturbances in the inner magnetosphere. The profile showed a large number of high-coherence events in the compressional component off the magnetic equator ($|\mathrm{Mlat}| > 30°$) on the nightside, even in the polar cap region. Teramoto et al. (2011) simultaneously investigated Pi2 pulsations in the inner magnetosphere on and off the magnetic equator, using magnetic field data from DE-1 and AMPTE/CCE. They reported that high-coherence events in the compressional component were only observed at a limited radial distance ($r < 7\ R_E$) at the magnetic equator, while they were frequently observed in high-latitude regions. These studies using polar-orbiting satellites have proposed that Pi2 pulsations are excited by the PVR mode.

As shown in previous studies using data from equatorial orbiting satellites and in numerical studies, the plasmasphere is an important region for the generation of mid- and low-latitude Pi2 pulsations. Although the latitudinal profiles of Pi2 pulsations in the magnetic field have been reported in a few previous studies, the relationship between high-coherence Pi2 pulsations off the equator and the plasmapause is not well specified because of a lack of electron density observations. Therefore, the wave properties of off-equatorial Pi2 pulsations relative to the plasmasphere are not clear. In addition, a recent study (Ghamry et al., 2015) showed that high-coherence

Pi2 pulsations appear at $L \sim 6$ near the nightside magnetic equator (|Mlat| < 11°) outside the plasmasphere (the plasmapause is located at $L \sim 5$), which is inconsistent with the PC mode suggested by statistical studies using equatorial orbiting satellites (Takahashi et al., 1995; Takahashi, Lee et al., 2003) and multi-satellite case studies (Collier et al., 2006; Luo et al., 2011). Further investigations on the spatial distribution of Pi2 pulsations at wider latitudinal and L ranges in the inner magnetosphere are needed. Thus, the present study investigates the spatial properties of Pi2 pulsations off the magnetic equator in relation to the plasmapause, using data from the Arase satellite, which has a unique orbit with an inclination of 31°. The unique inclination can encourage us to investigate off-equatorial Pi2 pulsations in the plasmasphere and in the vicinity of the plasmapause in more detail than the previous studies using the polar-orbiting satellite (Teramoto et al., 2008, 2011). The Arase satellite can remain around the plasmasphere for a longer time than the polar-orbiting satellites, which travel through the plasmasphere for only a short time due to their high inclination of ~90°.

The remainder of this paper proceeds as follows. Section 2 presents the dataset used. Section 3 provides the event selection and statistical results of the Pi2 pulsations observed by the Arase satellite. Section 4 discusses the relationship between the Pi2 pulsations and the plasmapause, and the generation mechanism of low-latitude Pi2 events. Finally, Section 5 summarizes and concludes the study.

2. Data Set

The Arase satellite is a spin-stabilized satellite that was developed by the Japan Aerospace Exploration Agency (JAXA) and launched on 20 December 2016 (Miyoshi, Shinohara, et al., 2018). It orbits in the inner magnetosphere with an apogee of 32,000 km and a perigee of ~400 km for altitude, which correspond to geocentric distances of 6.0 and 1.06 R_E, respectively, orbital period of 9.4 hr, and spin period of ~8 s. The Arase satellite can investigate off-equatorial Pi2 pulsations with a wide latitudinal range owing to its unique orbital inclination of ~31°. Arase occasionally can reach a dipole $L > 10$. We used spin-averaged magnetic field data with a time resolution of ~8 s from the magnetic field instrument (MGF, Matsuoka, Teramoto, Imajo, et al., 2018; Matsuoka, Teramoto, Nomura, et al., 2018), from 27 March 2017 to 27 September 2019. We adopted a local magnetic mean field-aligned coordinate system, where the z-axis of the B_P component is parallel to the mean background magnetic field of $<\boldsymbol{B}>$, the x-axis is perpendicular to $<\boldsymbol{B}>$ and radially outward (the B_R component), and the y-axis is perpendicular to $<\boldsymbol{B}>$ in an eastward direction (the $\boldsymbol{B}_A$ component). In this study, $<\boldsymbol{B}>$ is defined as the 5-min moving average of the observed magnetic field. To reduce the disturbance of the ambient magnetic field by much lower frequencies, we used B_P data, which were derived by subtracting the 5-min moving average B_P data from the measured B_P data. To identify the location of the plasmapause, we used the electron number density data observed by the High Frequency Analyzer (HFA, Kumamoto et al., 2018) of the Plasma Wave Experiment (PWE, Kasahara et al., 2018) onboard Arase, with a time resolution of 1 min. The electron number density was determined from the upper hybrid resonance waves.

To identify magnetic fluctuations in the inner magnetosphere that were highly correlated with Pi2 pulsations at low latitudes on the ground, we used the north–south (H) component of geomagnetic field data from three low-latitude ground stations, San Juan (SJG, 27.51° Mlat and 6.96° Mlon, $L \sim 1.27$), Honolulu (HON, 21.65° Mlat and 270.88° Mlon, $L \sim 1.16$), and Guam (GUA, 5.85° Mlat and 216.52° Mlon, $L \sim 1.01$). Because Pi2 pulsations at low latitudes dominantly appear in the H component, we examined the H component in this study. The H components of the geomagnetic field data at SJG, HON, and GUA have a 1-s sampling rate. After subtraction of the 300-s moving average, the residual geomagnetic field data (H) were downsampled for 8-s data to accommodate the MGF data.

The wave and planetary (Wp) index (Nosé et al., 2012; World Data Center for Geomagnetism, Kyoto & Nosé et al., 2016) was used to identify the onset times of the Pi2 pulsations. The Wp index was derived every minute by averaging the wavelet power of the 5.3–41.7 mHz frequency bands from 11 geomagnetic stations at low latitudes. These low-latitude geomagnetic stations with longitudinal separation were adopted so that at least one of the 11 stations would always be located on the nightside, where low-latitude Pi2 pulsations can be clearly observed.

10.1029/2021JA029677

3. Statistical Analysis of High-Coherence Events Observed by Arase

3.1. Identification of High-Coherence Events in the Magnetic Field Data

We identified high-coherence events, in which both ground stations and Arase observe the similar waveform of Pi2 pulsations, using the following two processes. In the first process, we select t_{Pi2} from the Wp index using two criteria: (a) the standard deviation of the Wp index for a 30 min time interval before t_{Pi2} should be less than 0.05 nT and (b) the Wp index should increase by more than 0.3 nT within 10 min after t_{Pi2}. The rapid increases in the Wp index identified by these two criteria indicate that low-latitude Pi2 pulsations appear on the ground at low latitudes. Because we wanted to focus on nightside low-latitude Pi2 pulsations at GUA, HON, and SJG, the selected t_{Pi2} was retained only when one of the three low-latitude ground stations was located on the nightside (21–03 MLT). Next, we visually assessed whether clear Pi2 pulsations are present in the geomagnetic field data from GUA, HON, and SJG at t_{Pi2}. Finally, we identified 1050 Pi2 events at the low-latitude ground stations at t_{Pi2} from 27 March 2017 to 27 September 2019.

In the second process, high-coherence events at t_{Pi2} were identified in the magnetic field data from Arase, using the same procedure as Teramoto et al. (2011). By applying the fast Fourier transform to 128 data points (∼17 min = 8 × 128 s), we calculated the power spectra of the geomagnetic field data in the H component and the magnetic field data in the B_R, B_A, and B_P components and automatically identified the peak frequency (i.e., the dominant frequency) from the H, B_R, B_A, and B_P power spectra. The coherence and cross phases of the B_R, B_A, and $\boldsymbol{B_P}$ components relative to the H component were also calculated. When the B–H coherence was > 0.7 at the common dominant frequencies, we regard the magnetic perturbations in the Arase data as high-coherence events. Pi2 pulsations in the inner magnetosphere have the multi-harmonic structure, indicating that the frequency of Pi2 pulsations contains both the fundamental and second harmonic frequencies (Lin et al., 1991; Takahashi, Anderson, & Hughes, 2003; Takahashi et al., 2018). In the first process, we detect the dominant frequency with the largest power of Pi2 pulsations at the low-latitude ground stations on the nightside, at which the power of Pi2 pulsations at the fundamental frequency is larger than that of Pi2 pulsations at the second harmonic frequency (Nosé, 1999; Takahashi, Anderson, & Hughes, 2003). Therefore, in this study, we detect Pi2 pulsations of the fundamental mode in the inner magnetosphere.

Figure 1 shows examples of high-coherence events in the B_P component that were selected using this process. The vertical dashed lines in Figure 1 indicate t_{Pi2}, which was automatically detected from the Wp index during the first process. Figure 1a shows that the Wp index starts increasing from ∼0.1 nT to ∼0.6 nT for 13 min after t_{Pi2}. Corresponding with the increase in the Wp index, clear Pi2 pulsations can be seen in the H component at SJG, with a period of ∼2 min, as shown in Figure 1b. Figures 1c–1e show the magnetic field data in the B_R, B_A, and B_P components from the Arase satellite, which was in the pre-midnight sector (∼21.4 MLT) off the magnetic equator (38.2° Mlat) at high L (L_m, McIlwain L in IGRF model, ∼8). Irregular magnetic perturbations occurred in the transverse (B_R and B_A) components, which do not resemble the Pi2 pulsations at SJG. In contrast, the magnetic perturbations in the B_P component had similar waveforms to the Pi2 pulsations at SJG with the same period (∼2 min). The peak-to-peak amplitude of the B_P magnetic perturbations (∼0.6 nT) was much smaller than that of the Pi2 pulsations (∼2 nT) at SJG. The B_P magnetic perturbations were also identified as having out-of-phase relationships with Pi2 at SJG.

The power spectra of the magnetic perturbations in the B_R, B_A, and B_P components of the Arase data are represented by thick lines in Figures 2a–2c. The dominant frequencies of the magnetic perturbations in the B_R, B_A, and B_P components were ∼7, 7, and 9 mHz, respectively. The gray lines in Figures 2a–2c show the power spectra of the Pi2 pulsations in the H component at SJG, as a reference. The H power spectrum had a clear peak at a dominant frequency of 9 mHz. Only the B_P component shared a dominant frequency with the Pi2 pulsations in the H component at SJG. The B_P power was larger by an order of magnitude than that of H at ∼9 mHz. Figures 2d and 2e show that the B_R-H and B_A-H coherences were very low across the whole Pi2 range (6.7–25 mHz). At 9 mHz, the B_P-H coherence was high (∼0.9), as shown in Figure 2f, indicating that the magnetic disturbance in the B_P component is a high-coherence event. Figures 2g, 2h, and 2i show the cross phases of B_R, B_A, and B_P relative to H, respectively. The cross phases were plotted when the coherences were > 0.7. The B_P-H cross phase was ∼180° at 9 mHz. Using this process, we successfully identified magnetic field perturbations that had high coherence with Pi2 pulsations at low-latitude ground stations.

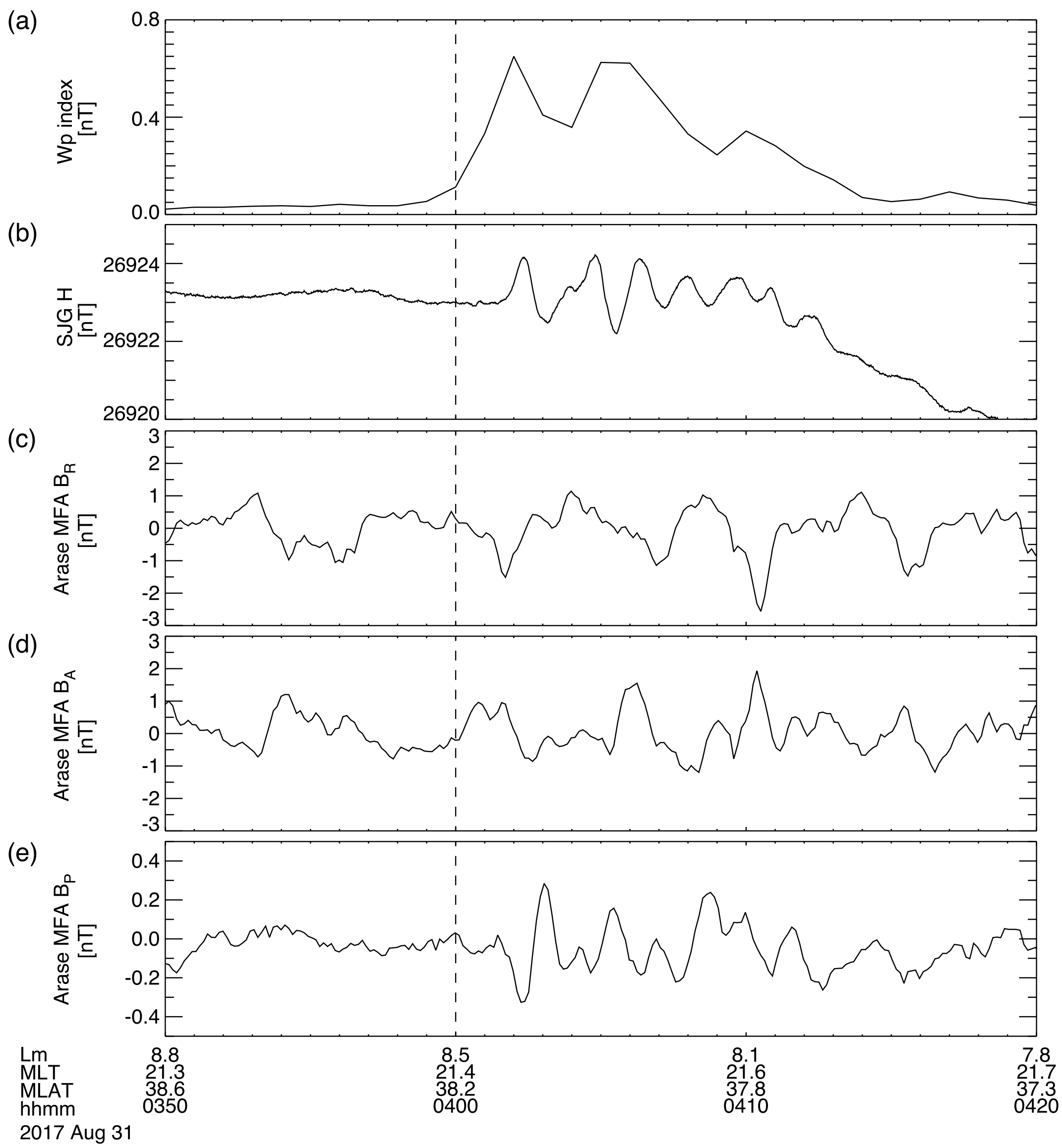

Figure 1. Example of a satellite-ground Pi2 pulsation event showing (a) the Wp index, (b) the waveform of Pi2 pulsations in the H component of the geomagnetic field at San Juan (SJG), and (c)–(e) the magnetic field components in the B_R (radial), B_A (azimuthal), and B_P (compressional) components in the local magnetic mean field-aligned coordinate system, observed by the Arase satellite. The dashed vertical line indicates the onset time of a low-latitude Pi2 pulsation on the ground, t_{Pi2}, which was identified using the Wp index.

3.2. Spatial Distribution and Number of High-Coherence Events

Figure 3a shows the MLT-L distribution of Arase locations when the 1050 nightside Pi2 pulsations were identified at low-latitude ground stations at t_{Pi2}. The red dots indicate that high-coherence events were detected in the magnetic field data of the Arase satellite for at least one component. The black dots show the low-coherence (< 0.7) events. Although the Arase observations cover a wide range of MLT and L at t_{Pi2}, high-coherence events were observed on the nightside (18–06 MLT). There were no high-coherence events on the dayside (07–15 MLT), which is consistent with previous statistical studies using satellite observations (Takahashi et al., 1995; Takahashi, Lee, et al., 2003; Teramoto et al., 2008, 2011). The nightside occurrence bias of high-coherence events implies that the source region of the low-latitude Pi2 pulsations was located on the nightside and not on the dayside. Figure 3b shows the $\sqrt{X_{SM}^2 + Y_{SM}^2} - |Z_{SM}|$ distribution of Arase locations on the nightside (18–06

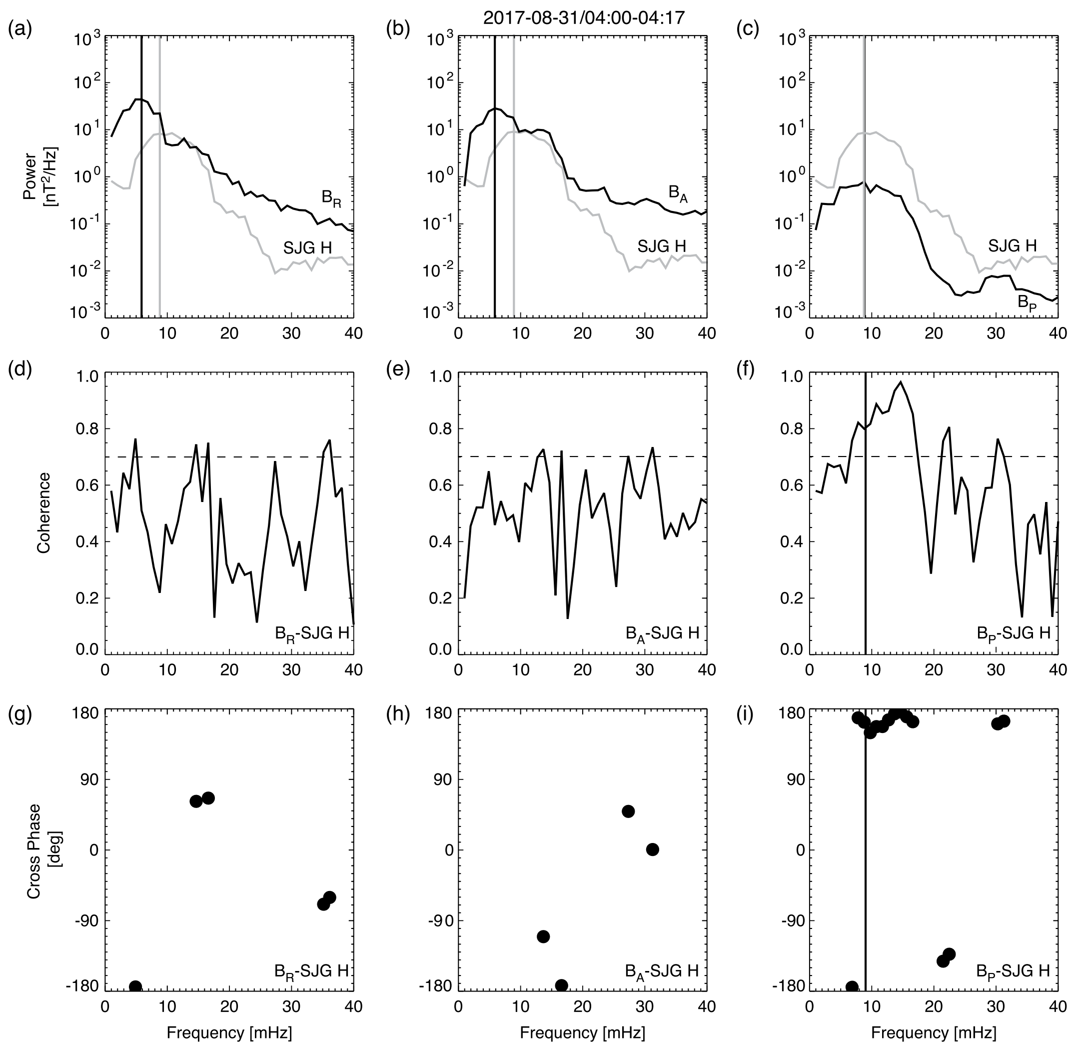

Figure 2. Spectral analysis of the Pi2 pulsations shown in Figure 1. The black lines indicate the power spectra of the magnetic fields in the (a) B_R, (b) B_A, and (c) B_P components. The power spectra of the geomagnetic fields in the H component at SJG are represented by gray lines in (a)–(c). The thick gray vertical lines represent the peak frequencies of the B and H power, respectively. The (d) B_R-H, (e) B_A-H, and (f) B_P-H coherences are shown. The horizontal dashed lines indicate coherence of 0.7. (g)–(h) The phase of the satellite relative to the ground is represented only for the frequencies at which the ground-satellite Pi2 pulsation coherence was > 0.7. The vertical lines indicate the peaks of the satellite and ground spectra.

MLT). Despite the Arase satellite being located off the magnetic equator (|Mlat| > 15°), high-coherence events on the nightside could be identified. The white and red histograms in Figure 3c represent the number of ground and high-coherence events as the function of log power of ground Pi2, respectively. Both ground and high-coherence events numbers are largest when ground Pi2 pulsations have the power of 1.0–10 nT^2/Hz. The numbers of the ground Pi2 events with lower (< 1.0 nT^2/Hz) and the largest (> 10 nT^2/Hz) power are comparable. The occurrence rate of Pi2 pulsations is shown by the blue line in Figure 3c. The occurrence rate increases as the log power of ground Pi2 increases, indicating that the occurrence rate of high-coherence events depends on the power of ground Pi2 pulsations.

The numbers of high-coherence events are presented in Figure 4. Of the 1,050 events, 154 (14%) showed high coherence in at least one field component. The number of high-coherence events was largest in the B_P component and smallest in the B_A component. The Arase satellite dominantly observed high-coherence Pi2 pulsations in the radial or compressional components, rather than the toroidal component. When the high-coherence events observed by Arase are associated with FLR (Keiling et al., 2001) and field-aligned propagating waves (Osaki et al., 1998), high-coherence events are frequently detected in the toroidal component. However, Arase

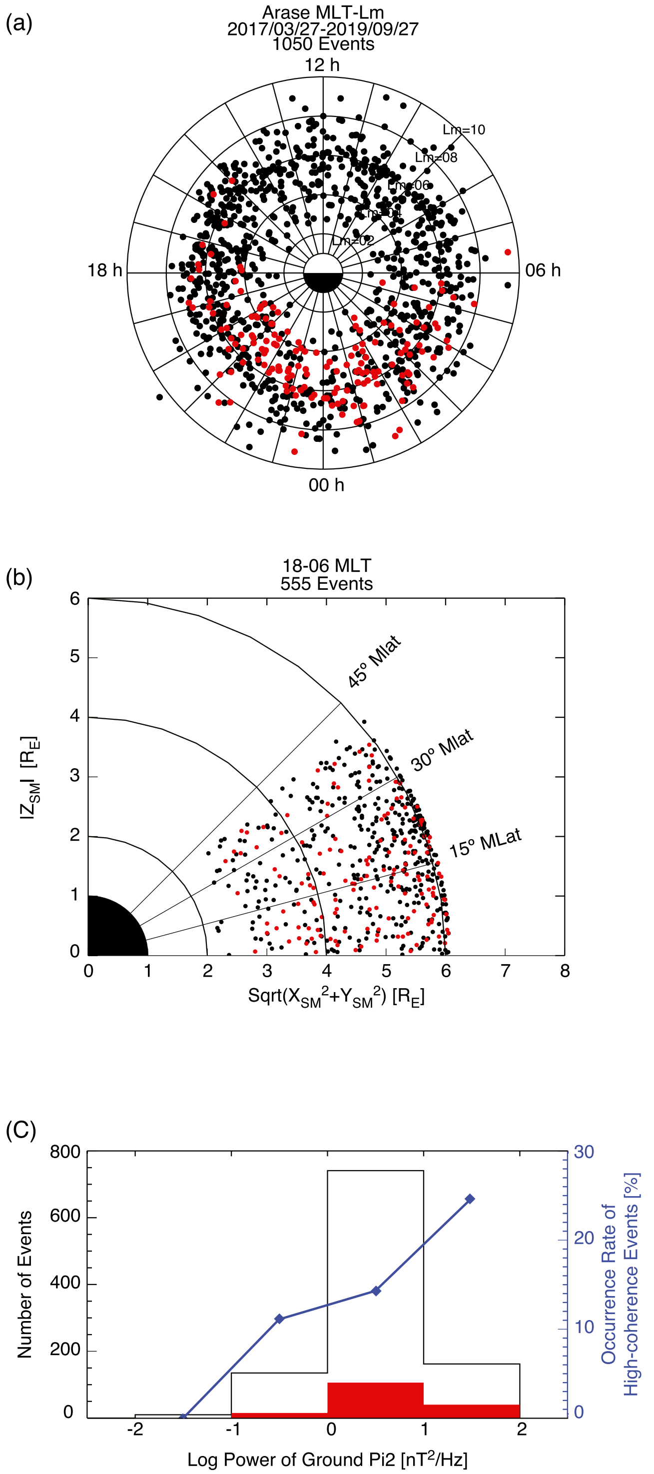

Figure 3. (a) MLT–L_m and (b) $sqrt(X^2_{SM} + Y^2_{SM})$–$|Z_{SM}|$ distributions of the Arase locations at t_{Pi2}. The red and black dots show high- and low-coherence events observed by Arase, respectively. (c) The number of all events (the white histogram) and the high-coherence events (the red histogram) as a function of the power of ground Pi2 pulsations. The occurrence rate of high-coherence events is represented by a blue line.

observations indicate that low-latitude Pi2 pulsations originate from poloidal mode waves, particularly from fast mode waves, which is inconsistent with the FLR mode. The Arase observations are consistent with the statistical studies using data from the polar-orbiting DE-1 satellite by Teramoto et al. (2008, 2011). In the following analysis of high-coherence events, we show the results of the B_R and B_P high-coherence events, which were the dominant components.

3.3. MLT-Mlat Dependence of Occurrence Rate and Power Ratio

In Figure 5, we show the MLT-|Mlat| distributions of high-coherence events in the radial B_R and compressional B_P components. Figure 5a shows the MLT-|Mlat| distribution of the cumulative Arase observation time and the number of ground Pi2 pulsations. The Arase satellite spends a large amount of time at mid-latitudes (15°–30°|Mlat|); its cumulative time spent at high latitudes (30°–45°|Mlat|) is only half that spent at mid-latitudes. To quantify the occurrence rate of high-coherence events on the nightside, we calculated the occurrence rate by dividing the number of high-coherence events by the number of Pi2 events on the ground in each bin. The occurrence rate distribution of the high-coherence B_R events is shown in Figure 5b. The rate is higher at low latitude (|Mlat| = 0°–15°) than at mid or high latitudes (|Mlat| > 15°), indicating that the poloidal mode waves are confined to the magnetic equator. However, Figure 5c shows that high-coherence B_P events were observed with a wider latitudinal range than the B_R events. The occurrence rates of the high-coherence B_P events in the 20–02 MLT sector were ∼27% in average, in a wider latitudinal range of 0°–45° which were higher at any Mlat or MLT value than that of the corresponding high-coherence B_R events. The occurrence rates shown in Figures 5b and 5c have high degree of variability from one bin to another. This is because the number of events is not uniform in each bin as shown in Figure 5a. Although the number of events has latitudinal dependence, in which the number of events at high latitudes is smaller than those at mid and low latitudes, the number of events has no significant MLT dependence. Not only the occurrence rate but the number of high-coherence events is larger at 20–02 MLT sectors than in other sectors. Figures 5b and 5c also show that both the high-coherence B_R and B_P events frequently appear in the 20–02MLT sector in the magnetic equatorial region.

Figures 6a and 6b show the MLT dependence of the satellite-to-ground power ratio, with the lines indicating the average value in each 2-hr MLT range. The black, green, and red colors represent the high-coherence events for three Mlat bins, the low (|Mlat| = 0°–15°), mid (|Mlat| = 15°–30°), and high (|Mlat| = 30°–45°) latitudes, respectively. The average value of the B_R-H power ratio at high latitudes is not shown because there were not enough high-coherence events to average. The averaged B_R-H power ratios show no clear MLT dependence in the pre-midnight sector (20–02 MLT) at either low- or mid-latitudes, while the averaged B_P-H power ratios at low and mid latitudes showed maxima at 23 and 21 MLT (pre-midnight), respectively. To assess the significance of the maxima, we conducted unpaired t-tests between the adjacent MLT bins and the maximum MLT bins. The P values of the low-latitude 22–23 MLT and 23–00 MLT comparisons and the mid-latitude 20–21 MLT and 21–22 MLT comparisons were 0.34, 0.06, 0.24, and 0.26, respectively. The large P values (> 0.05) indicate no significant differences between the adjacent and maximum MLT bins in the statistical unpaired t-test. Although there were no significant differences between adjacent bins, the results seem to indicate B_P-H power enhancements in 20–02 MLT sector

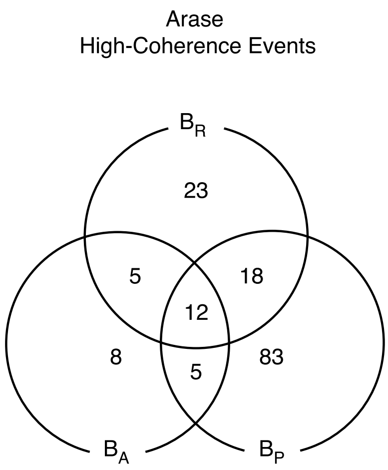

Figure 4. The number of high-coherence events observed by the Arase satellite.

at mid and low latitudes. Figures 6c and 6d indicate the MLT dependence of the satellite-to-ground power ratio for the low L_m ($L_m \leq 6$) and high L_m ($L_m > 6$), represented by the black and red colors. The vertical bars indicate the standard errors of the power ratio every 2-hr MLT bin. While the B_R-H power ratio at $L_m \leq 6$ has no MLT dependence, the B_P-H power ratio at $L_m \leq 6$ and $L_m > 6$ has a maximum at 23 MLT. The B_p-H power enhancements in 20–02 MLT sector also are seen at $L_m \leq 6$ and $L_m > 6$.

3.4. L_m-Mlat Dependence of Occurrence Rate for Nightside Events and Mlat Dependence of Power Ratio

Figure 7 shows the cumulative time of the Arase satellite, the number of ground Pi2 pulsations, and the occurrence rate of B_R and B_P high-coherence events, as a function of |Mlat| and L_m, in the pre-midnight sector (20–02 MLT), in which the occurrence probability was high, as shown in Figure 5. Because of orbital restrictions, Arase observations are entirely absent at high–L_m and low- and mid-latitudes in the (L_m, |Mlat|) bins of (6–10, 0°–15°) and (8–10, 15°–30°), respectively. The Arase spent most of its time at an L_m of 6–7 at a mid-latitude of 15°–30° |Mlat|. In the high-latitude (30°–45° |Mlat|) and high L_m (6–10) bins, no high-coherence events were observed in the B_R component, whereas high-coherence B_P events appeared with a moderate occurrence rate of ∼20%. High-coherence B_R events were frequently observed in the near-Earth region ($L_m < 6$) at all magnetic latitudes. In contrast, the high-coherence B_P events appeared over wide L_m and |Mlat| ranges, which is consistent with the previous studies using polar-orbiting satellites by Teramoto et al. (2008, 2011). At low latitudes (0°–15° |Mlat|), high-coherence B_P events were detected even at $L_m > 4$, with an occurrence rate > 30%. The low-latitude occurrence rate in the B_P component increased earthward, except at L_m ∼3–4. The maximum occurrence rate of the high-coherence B_P events was ∼66% at low-latitude and L_m ∼2–3, but it is noted that the number of ground Pi2 pulsations events is very small (3) as shown in Figure 7a. The occurrence rate of B_P at L_m ∼3–4 is low although there are a high enough number of events (more than 10). In contrast, the occurrence rate of the B_R component in the 0°–15° |Mlat| and 03–04 L_m bin is much higher occurrence rate (∼41%) than the B_P component in the same bin. We will explain these properties from the point of view of the PVR nodal structure in discussion section.

We investigate the |Mlat| distributions of the B_R-H and B_P-H power ratios for the nightside high-coherence events (Figure 8). The B_R-H power on a logarithmic scale increased monotonically with increasing latitude. The linear correlation coefficient for B_R events was 0.62 and the slope was 0.031. A similar positive correlation for the B_R-H power ratio was reported by Takahashi et al. (1995) while their observations are limited near the magnetic equator (|Mlat| < 15°). Considering the latitudinal structure of poloidal waves, the amplitude of poloidal mode waves increases with increasing magnetic latitude because the fundamental poloidal oscillations have nodes and antinodes on and off the magnetic equator, respectively. The positive correlation of the B_R-H power ratio implies that poloidal mode waves with symmetrical modes are excited. In contrast to the B_R-H power distribution, the B_P-H power ratio decreases monotonically with increasing latitude, with a high correlation coefficient of −0.63.

Considering the latitudinal structure of the PVR mode, the amplitudes of B_R and B_P have latitudinal dependence within the plasmasphere. According to 3D simulations of the PVR mode, the B_R component has a node at the magnetic equator, and the B_R amplitude increases with latitude. The amplitude of the B_P component is largest at the magnetic equator in the plasmasphere and decreases with increasing latitude. Both the B_R and B_P power ratio distributions shown in Figure 8 are consistent with the PVR mode structure. Takahashi et al. (1995) showed a positive correlation between latitude and the B_R-H power ratio using AMPTE/CCE observations near the magnetic equator (< 15° |Mlat|). However, the power ratio of the B_P components did not depend on the magnetic latitude. We investigated the Mlat dependence of B_P-H power ratio near the magnetic equator (< 15° |Mlat|) of Arase observations (see Text S1 and Figure S1 in Supporting Information S1) and found that the correlation coefficient between |Mlat| and the B_P-H power ratio is low (−0.01). The high Mlat dependence of the B_P-H power ratio is seen when the observational region includes higher latitudes. To confirm that the Mlat distribution of the B_P-H power ratio in Figure 8b is independent of L_m, we investigated the Mlat distribution of the B_P-H power ratio with a limited L_m of 4.5–5.5 and 5.5–6.5 (see Text S2 and Figure S2 in Supporting Information S1). Although the L_m

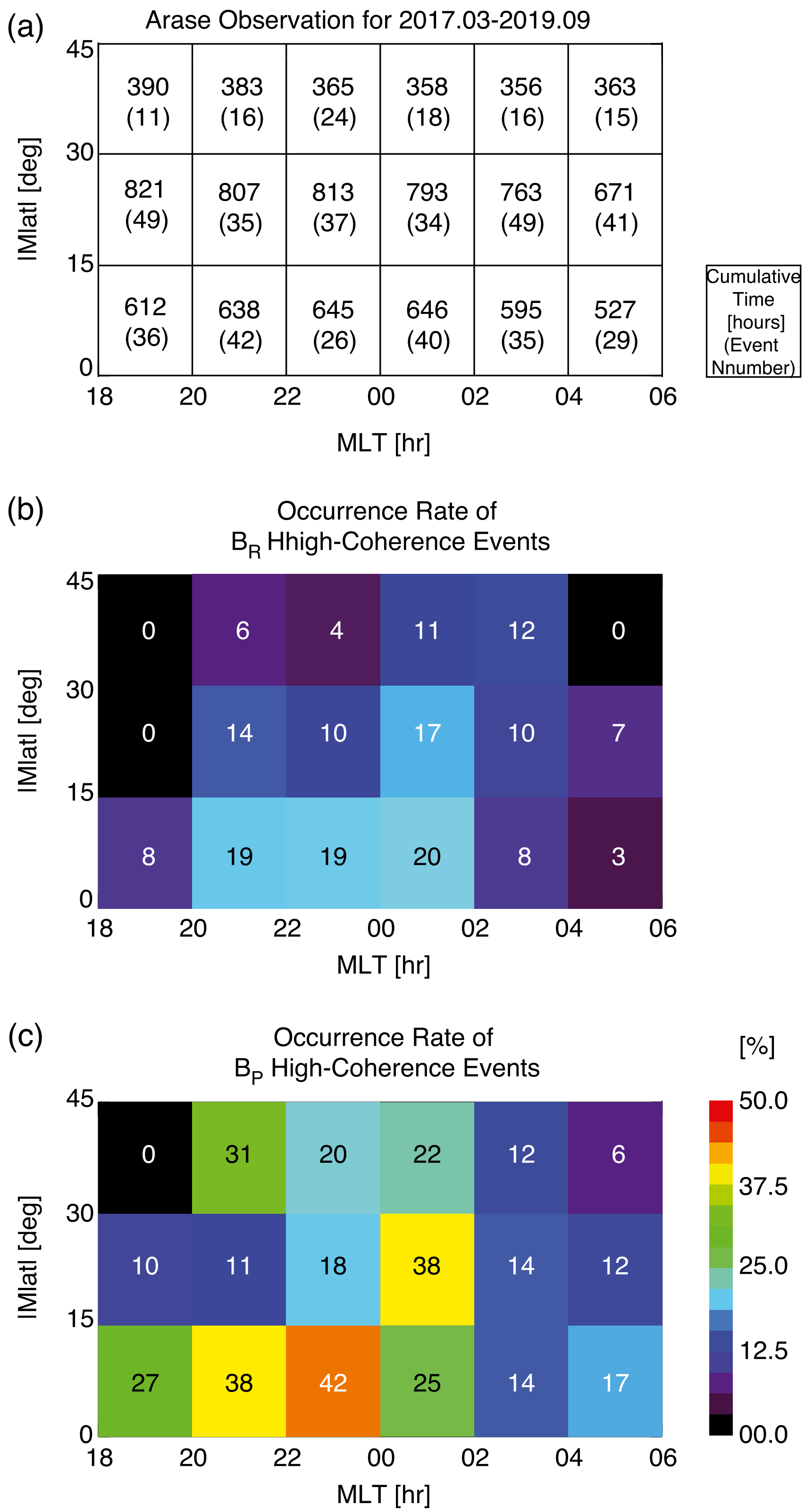

Figure 5. MLT-Mlat distributions of (a) the cumulative time of the Arase satellite and (b)–(c) the occurrence rate of high-coherence events in the B_R and B_P components. Occurrence probability was defined as the number of high-coherence events divided by that of t_{Pi2} events in each |Mlat| and MLT bin.

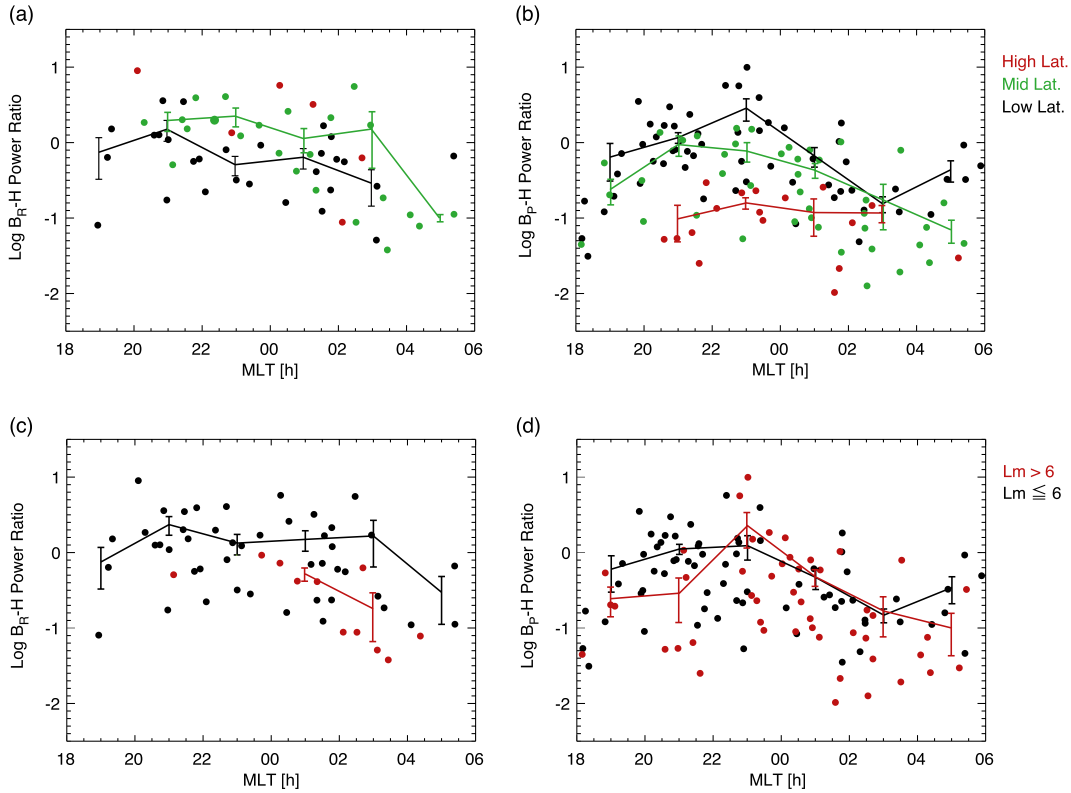

Figure 6. MLT dependence of the log (a) B_R-H and (b) B_P-H power ratios for high-coherence events. The black, green, and red colors indicate low- (|Mlat| < 15°), mid- (15° < |Mlat| < 30°), and high-latitude (30° < |Mlat| < 45°) events. The lines indicate the average log power ratio for each 2-hr MLT bin. The vertical bars indicate the standard errors for each 2-hr MLT. The average log B_R-H power ratios at high latitudes are not shown owing to the small number of high-coherence events. MLT dependence of (c) B_R-H and (d) B_P-H power ratios for high-coherence events with dividing the high-coherence events to two categories of high ($L_m > 6$) and low ($L_m \leq 6$) L_m. The low and high L_m are represented by black and red colors. The average log power ratio and the error bars are represented by the same format as Figures 6 (a) and (b).

was limited, moderate negative correlations (−0.52 and −0.47) were observed between Mlat and the B_P-H power ratio. These results indicate that the Mlat dependence shown in Figure 8 is not affected by the L shell. Using multiple-satellite observations from the CCE and DE-1, Teramoto et al. (2011) indicated that the B_P-H power ratio decreased by a factor of ∼3 from the equatorial plasmasphere (∼0° Mlat) to the polar cap (∼90° Mlat). The negative trend shown in Figure 8b is consistent with the results by Teramoto et al. (2011). In this study, the factor is ∼1.3 from the magnetic equator to the off-equatorial region at ∼40° |Mlat|.

3.5. Plasmapause Dependence

To investigate the amplitude and phase properties of high-coherence events relative to the plasmapause, we examined the electron density observed by PWE/HFA and determined the plasmapause location (L_{pp}) whenever the Arase satellite identified at least one high-coherence Pi2 event in the pre-midnight sector (20–02 MLT). To reduce the MLT dependence of the L shell in this analysis, we used the McIlwain L calculated in the Tsyganenko 04 model (Tsyganenko & Sitnov, 2005) by tracing particles with a 90° pitch angle. Automatically, we defined the plasmapause-crossing timing, at which the electron number density drops or increases with more than a factor of 10 and the L_m difference is smaller than 0.5 for 5 min. We also checked that the plasmapause locations were successfully identified by the visual inspection. The inner edge of the steep gradient was regarded as the L_{pp}. Because the L_{pp} value differs between the outbound and inbound passes of the same orbit, we chose the L_{pp} with an MLT closer to the location of the high-coherence events observed by Arase in the same orbit. We note that the plasmapause identified by the total mass density is different from the plasmapause identified by the electron number density. The plasmapause of the total mass density is located at one or two higher L shells than the plasmapause

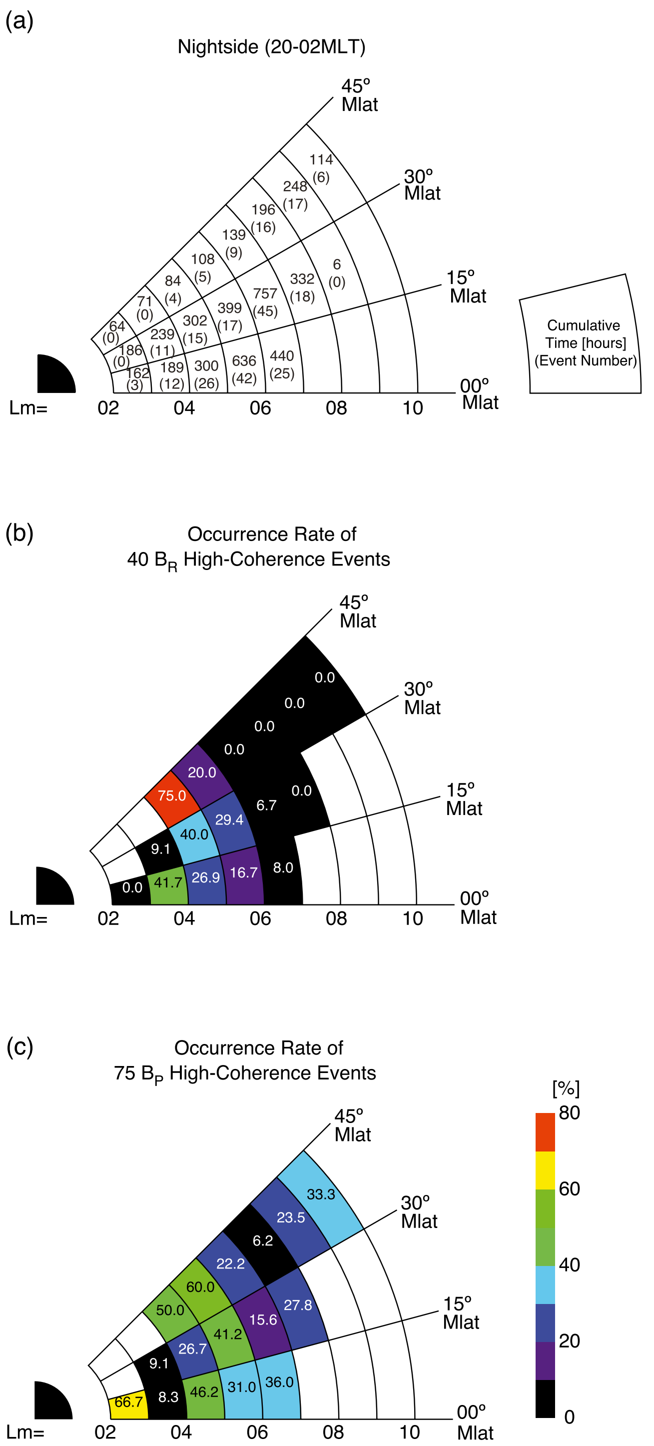

Figure 7. L_m–|Mlat| distributions of (a) the cumulative time of the Arase satellite and (b)–(c) the occurrence rate of high-coherence events in the B_R and B_P components.

of the electron number density if the oxygen torus is formed outside the plasmapause identified by the electron number density (Nosé et al., 2018, 2020; Takahashi et al., 2008). Although the structure of Pi2 pulsations in the inner magnetosphere is affected by the total mass density rather than the electron number density, we use the electron number density to identify the plasmapause. It is because identification of the plasmapause from the electron number density is much easier than investigation of the total number density, in which we need the analysis of the ULF waves with the FLR structures. As an example, Figure 9 shows the electron density on the Arase orbit that includes the B_P event shown in Figure 1, which occurred outside the plasmasphere (highlighted by hatching). For some high-coherence events, we could not define L_{pp} because there was a gradual change in the electron density without a steep gradient. The L_{pp} was available in 28 out of 40 (70%) in the B_R component and 57 (76%) of 75 events in the B_P component.

Figure 10 shows the ΔL distributions of the log power ratios and cross phases of the B_R and B_P components, relative to the H component, for the high-coherence nightside events. The relative plasmapause distance was defined as $\Delta L = L_m - L_{pp}$. $\Delta L < 0$ indicates that high-coherence events were detected in the plasmasphere. The open and filled circles represent the northern ($Z_{SM} <$ 0) and southern ($Z_{SM} > 0$) observations, respectively. The lines in Figures 10a and 10b indicate the average power ratio values per 1-ΔL bin. The vertical vars indicate the standard errors at 1–ΔL bin. To reduce the Mlat bias of the Arase orbit, the log power ratio in Figures 10a and 10b is mapped to 0° |Mlat|, using the |Mlat| dependence of power ratio in Figures 8a and 8b. Figure 10a reveals a nearly constant B_R-H power ratio in the vicinity of the plasmapause ($|\Delta L| < 1$), with high-coherence B_R events confined to $\Delta L < 1$. In contrast, the B_P-H power ratio likely exhibits a peak near the plasmapause at $\Delta L \sim 0$ with the wider spread outside the plasmapause ($\Delta L > 1$). Figure 10c shows that the B_R-H cross phases cluster around ∼0° and ∼180° in the northern and southern hemispheres, respectively. This distribution indicates that high-coherence B_R events have a symmetrical pattern with respect to the equator. Irrespective of hemisphere, the B_P-H cross-phase distribution (Figure 10d) shows an in-phase relationship inside the plasmasphere ($\Delta L < -1$), the phase change from 0° to 180° in the vicinity of the plasmapause ($-1 < \Delta L < 0$), and the out-of-phase relation outside the plasmapause ($\Delta L > 1$). These B_P-H and B_R-H cross-phase structures were predicted by a PVR mode simulation using an magnetohydrodynamic code (Lee & Takahashi, 2006), as shown in Teramoto et al. (2011). Teramoto et al. (2011) reported the ΔL distributions of B_P-H cross phases using multiple observations from the polar-orbiting DE-1 and AMPTE/CCE satellites. However, the distributions showed no sharp changes and large variation because the plasmapause was identified using an empirical model from the Kp index. In this study, we identified the L_{pp} using electron density data from PWE/HFA. Thus, a clear B_P–H phase change could be seen in the vicinity of the plasmapause ($\Delta L \sim 0$), as predicted by numerical simulations of the PVR mode. Figures 10e and 10d show ΔL distributions of |Mlat| of high-coherence events in the B_R and B_P components, respectively. The 13 events out of B_R-H high-coherence events were observed at mid and high latitudes (>15° |Mlat|). Most of B_P-H high-coherence events with ∼180° cross phase at $\Delta L > 2$ are observed off the magnetic equator (< 15° |Mlat|). Although high-coherence B_R events are observed at higher latitude (> 15° |Mlat|), the observational region is limited in the vicinity of the plasmapause ($\Delta L < 1$). In contrast, high-coherence B_P events are present at higher latitudes (> 15° |Mlat|) with a long distance from the plasmapause ($\Delta L > 2$). This result indicates that the high-coherence B_R events are confined in the vicinity of the plasmapause

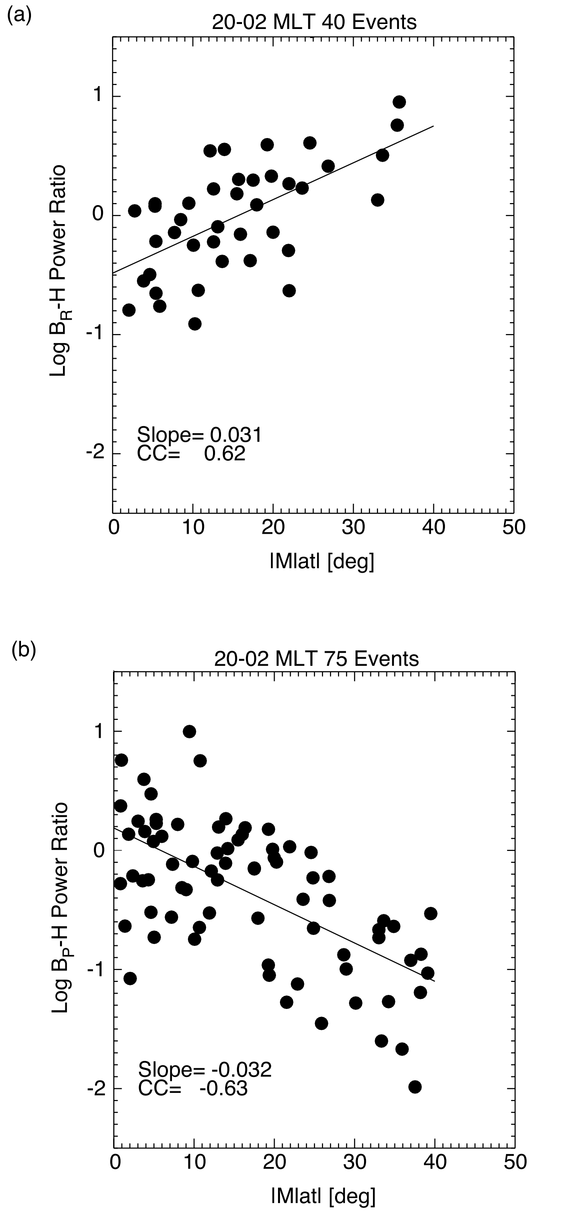

Figure 8. |Mlat| dependence of the log (a) B_R-H and (b) B_P-H power ratios of nightside high-coherence events. The straight lines indicate the linear regression analysis of each scatter diagram. The slope of the line and linear correlation coefficient between the magnetic latitude and power ratio are shown.

while the high-coherence B_P events are present within the wide region off the magnetic equator beyond the plasmapause.

4. Discussion

In this study, we show the spatial properties of the occurrence rate of high-coherence events, and the ΔL distributions of the power ratios and cross phases of the B_R and B_P components relative to the H component, to investigate the generation mechanism of low-latitude Pi2 pulsations.

Figure 3 shows that high-coherence events were frequently observed on the nightside while there were no high-coherence events on the dayside (07–14 MLT). Of the 154 high-coherence events, 118 appeared in the B_P component. In the off-equatorial inner magnetosphere, the compressional component dominated the magnetic disturbances with high coherence to low-latitude ground Pi2 pulsations, which has already been reported in previous statistical studies using polar-orbiting satellite data (Teramoto et al., 2008, 2011). The occurrence rate of high-coherence B_P events was especially high in the pre-midnight sector. B_P-H power ratio enhancement was evident in the 20–02 MLT sector at low and mid-latitudes (|Mlat| < 30°). This result is consistent with the longitudinal power distributions of Pi2 pulsations in the H component observed by low-latitude ground stations during substorm (Takahashi & Liou, 2004) and quiet periods (Kwon et al., 2013). Similar dawn-dusk asymmetry in the MLTs of occurrence rate or power distributions is also seen in the other substorm-related phenomena, such as injections (Gabrielse et al., 2014; Sergeev et al., 2012), fast flows in the plasma sheet (McPherron et al., 2011; Runov et al., 2005), and dipolarizing flux bundles (Liu et al., 2013). The MLT distributions indicate that the source regions of the Pi2 pulsations are in the pre-midnight sector. In both the BBF and PC/PVR modes of low-latitude Pi2 pulsation generation, the source region is expected to be located in the pre-midnight sector. The asymmetrical MLT power and occurrence rate distributions support a pre-midnight source of low-latitude Pi2 pulsations.

Previous statistical studies of off-equatorial Pi2 pulsations using polar-orbiting satellites reported that high-coherence Pi2 pulsations were most often detected in the compressional component, rather than in the transverse components (Teramoto et al., 2008, 2011). Consistently, the Arase observations show a higher number of high-coherence events in the compressional B_P component than in the transverse B_R and B_A components. However, high-coherence B_R events were detected more frequently in the Arase observations than in the polar-orbiting DE-1 observations in Teramoto et al. (2008, 2011). The observation ratio of B_R events to B_P events was ~50% in this study, while the ratio were 33% and 24% in the study by Teramoto et al. (2008, 2011), respectively. Considering the spatial distributions of the radial and compressional components in the PVR mode, we can explain this difference in the B_R-B_P observation ratio between Arase and DE-1. In the PVR mode simulation presented by Teramoto et al. (2011), Pi2 pulsations in the compressional component exist over a wider latitudinal range beyond the plasmapause than those in the radial component. Consistently, Figures 7b and 7c show that the high-occurrence region of high-coherence B_R events is confined to $L_m < 6$, while that of high-coherence B_P events spreads across the high-latitude area at $L_m > 6$. Numerical simulations of the PVR mode also show that Pi2 pulsations in the radial component exist in the off-equatorial plasmasphere and in the vicinity of the off-equatorial plasmapause. Owing to its orbital inclination of 31°, the Arase satellite spends much more time in the vicinity of the off-equatorial plasmapause than polar-orbiting satellites. Therefore, Arase can observe Pi2 pulsations in the B_R component more frequently than a polar-orbiting satellite, which would stay in the polar region most of the time. Such comprehensive investigation of off-equatorial Pi2 pulsations in both of the radial

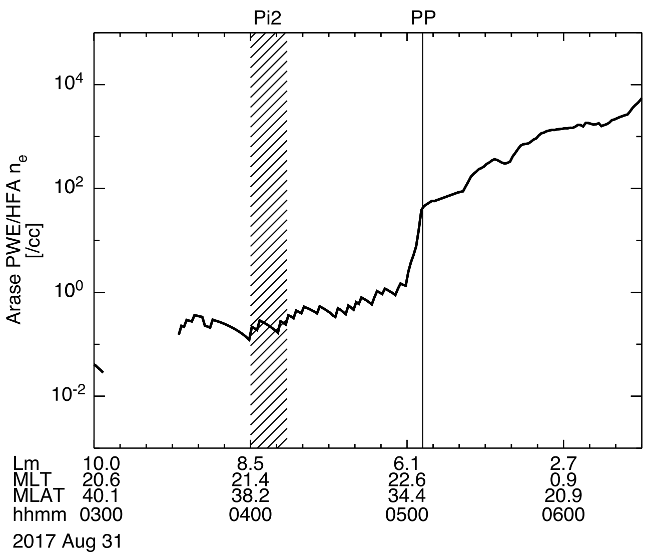

Figure 9. Time series of electron density data observed by HFA/PWE when Arase observed the high-coherence Pi2 event shown in Figure 1. The diagonally shaded region represents the period of the high-coherence event observation by Arase. The vertical line indicates the plasmapause (PP) used in this study.

and compressional components is not reported by previous statistical studies using a polar-orbiting satellite (Teramoto et al., 2008, 2011). As further support for the latitudinal properties of the radial component in the PVR mode, Figures 7b and 8a show that the amplitude and occurrence rate at $L_m \sim 4$–5 of high-coherence B_R events increase with increasing latitude.

In this study, we obtained the ΔL dependences of the power ratios and cross phases of the high-coherence B_R and B_P components, relative to the H component, at the low-latitude ground stations on the nightside. The ΔL distributions of the high-coherence B_R and B_P events shown in Figure 10 are also consistent with the PVR mode. First, we considered the ΔL distributions of the B_R-H power ratio and phase. The B_R-H power ratio is almost constant in the plasmasphere and in the vicinity of the plasmapause ($-2 < \Delta L < 1$). According to the PVR mode simulation in Teramoto et al. (2011), the radial component of PVR oscillation has a node at the magnetic equator and antinodes in both hemispheres. In particular, the regions of amplitude enhancement in the radial component (i.e., antinode regions) extend into the off-equatorial plasmasphere and in the vicinity of the off-equatorial plasmapause. The constant distribution of the B_R-H amplitude ratio shown in Figure 10a is likely to correspond to the spatial expansion of the amplitude enhancement in the radial component in the PVR mode. Considering the field line displacement pattern of the eigenmode in the plasmasphere represented by Takahashi et al. (1995), the radial magnetic field displacements in the southern and northern hemispheres are in the opposite direction. The B_R-H cross-phase distribution shown in Figure 10c agrees with the phase distribution of the radial component in the PVR mode.

Next, we considered the ΔL distributions of the B_P-H power ratio and the cross phase using Pi2 pulsations observed off the equator. According to previous studies showing ΔL distributions of Pi2 in the equator, the B_P-H power ratio likely has a gradual peak at the plasmapause ($\Delta L = 0$). When an eigenmode is excited anywhere in the plasmasphere, the amplitude of the oscillations in the compressional component has a node in the plasmasphere and antinodes at the inner and outer boundaries of the ionosphere and plasmapause. The peak in the B_P-H power ratio at $\Delta L = 0$ shown in Figure 10b is consistent with the structure of the amplitude in the compressional component of the PVR mode, in which an antinode is located at the plasmapause. In a realistic magnetic field, the node is located so close to the outer boundary of the plasmapause that it could be difficult to clearly identify the nodal point using satellite observations, as shown in Figure 10b. Figure 7c shows that the occurrence rate of high-coherence B_P events is low at L_m of 3–4. This region could be related to the nodal point of the compressional component in the PVR mode, in which Pi2 pulsations are difficult to observe by satellite owing to their small amplitude. In the PVR mode, the magnetic fields between a nodal point and boundary oscillate in the same radial direction. Therefore, when the magnetic fields between the ionosphere and a nodal point become dense, those between the nodal point and the plasmapause become sparse. This means that the phase is changed from 0° to 180° at the nodal point, maintaining the same phase between the nodal point and the boundary. Consistently, the ΔL distribution shows that the B_P-H cross phases are ~0° and ~180° at $\Delta L < 0$ and $\Delta L > -2$, respectively, regardless of hemisphere. Most of the high-coherence B_P events outside the plasmasphere, that have out-of-phase relationships with the Pi2 pulsations on the ground, were observed off the equator (|Mlat| < 15°). In the PVR mode, the oscillation phase in the compressional component outside the plasmasphere is out-of-phase relative to the low-L Pi2 pulsations. The ΔL distributions of the B_P-H power ratio and cross phase in this study suggest the possibility that the PVR mode is excited even further from the magnetic equator in the inner magnetosphere.

Our observations show that the high-coherent Pi2 pulsations in the compressional component are observed in the vicinity of the plasmapause ($\Delta L < 1$) at the magnetic equator (|Mlat| < 10°) while high-coherence B_P events are detected beyond the plasmapause ($\Delta L > 1$) at high latitudes. This result may indicate that Pi2 pulsations excited by the PVR mode are spread off the magnetic equator. The previous statistical study (Takahashi, Lee, et al., 2003), which investigates the relationship of Pi2 pulsations to the plasmapause, showed that the compressional Pi2 pulsations in the magnetic field around the magnetic equator (|Mlat| < 13°) are confined within the

10.1029/2021JA029677

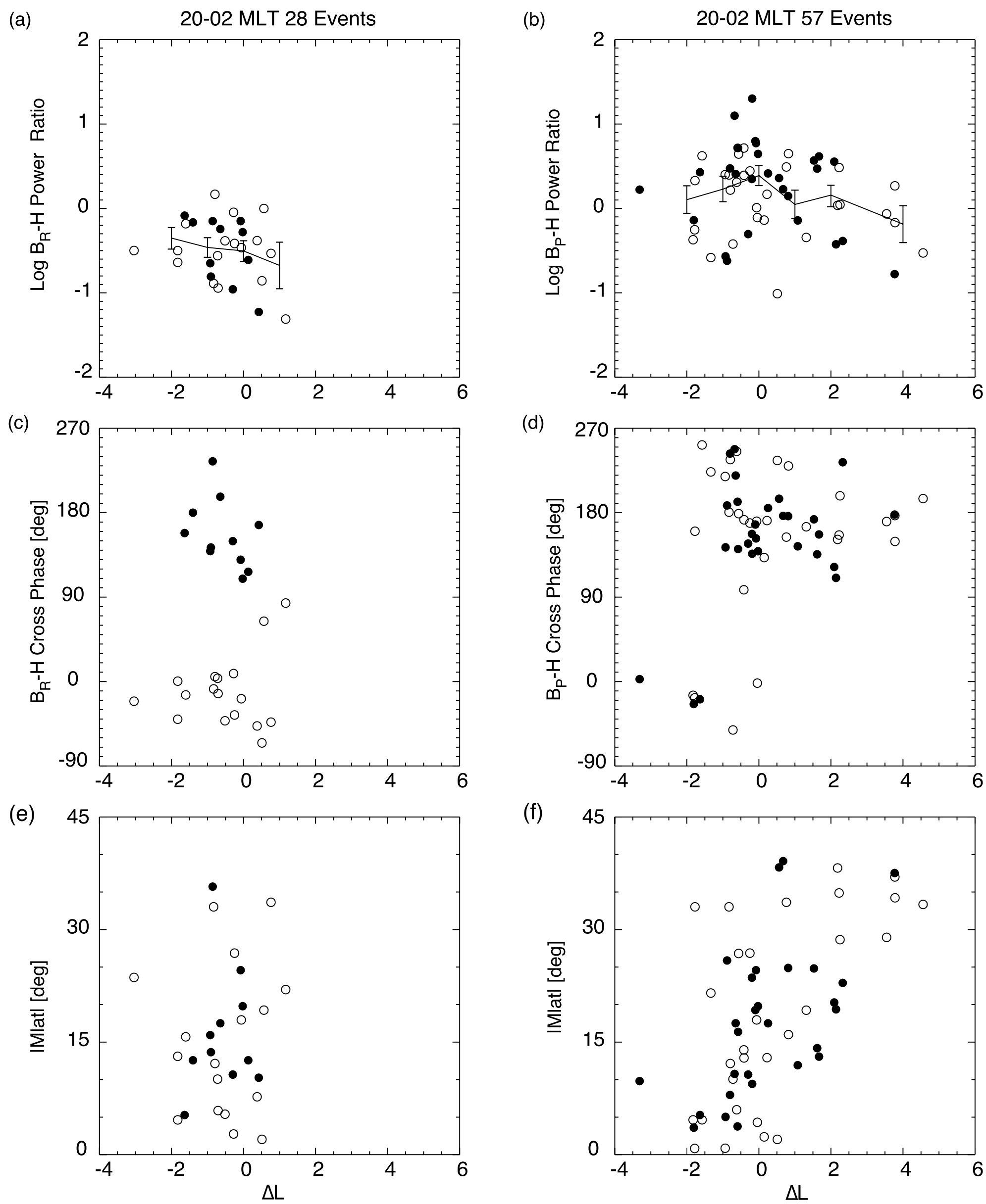

Figure 10. (a)–(b) power ratio, (c)–(d) cross-phase, and (e)–(f) |Malt| distributions versus ΔL for nightside B_R and B_P high-coherence events. The open and solid circles represent Arase observations in the northern and southern hemispheres, respectively. The black lines and vertical bars in (a) and (b) indicate the average power ratio and standard errors per ΔL bins.

plasmasphere. This result is consistent with our result shown in the distributions in low latitudes (|Mlat| < 10°). Our observations indicate that high-coherence events are spread wider, in regions beyond the plasmapause at high latitudes (|Mlat| > 10°), rather than at low latitudes (|Mlat| < 10°) in the inner magnetosphere. Multipoint observations of equatorial Pi2 pulsations on the nightside using the Time History of Events and Macroscale Interactions during Substorms (THEMIS) satellite (Luo et al., 2011) showed that the poloidal Pi2 pulsations with high coherence to low-latitude ground Pi2 pulsations are observed in the plasmasphere by the THEMIS-A and -E satellites while THEMIS-D satellite could not observe high-coherence events in the magnetic and electric fields outside the plasmapause at the magnetic equator (~3° Mlat). On the other hand, the resent multipoint observation using Van Allen Probes (Probe-A and -B) in Ghamry et al. (2015) showed that high-coherence compressional events are simultaneously observed inside and outside the plasmapause by the Probe-B and-A, respectively. Consistent with our results, the compressional high-coherence events outside the plasmapause in Ghamry et al. (2015) also have the out-of-phase relation to Pi2 pulsations at the low-latitude ground station of Bohyun

(BOH) when Probe-A and BOH was located at 0055MLT and 0300 MLT, respectively. When the high-coherence compressional events in Ghamry et al. (2015) are found outside the plasmapause ($\Delta L \sim 1$), the magnetic latitude of the Probe-A (∼−10.8° Mlat) is located at higher magnetic latitudes than the THEMIS-D. The ΔL distribution of the high-coherence B_P events is consistent with both multipoint observations of the Probe-A and THEMIS-D. Our observations may suggest that the high-coherence events of the compressional components associated with the PVR mode are detected outside the plasmasphere more easily off the equator (> 10° |Mlat|) than around the magnetic equator (< 10° |Mlat|).

We discuss our results with the properties expected from the direct BBF-driven model. If most of the high-coherence Pi2 pulsations identified in this study were directly excited by periodic BBFs, the occurrence rate in the higher L region would be higher than or comparable to that in the lower-L region because, in this mode, the source energy propagates from the boundary layer at $L > 8$ in the braking region. However, in this study, the occurrence rate of the high-coherence B_P events was low in the high L shell ($L_m > 6$), and the high-occurrence (> 40%) region of the B_P component was in the near-earth region ($L_m < 6$). These results are consistent with those of previous studies using equatorial-orbiting (Takahashi et al., 1995; Takahashi, Lee, et al., 2003) and polar-orbiting satellites (Teramoto et al., 2008, 2011). The enhancement of the B_P occurrence rate at $L_m < 6$ indicates that the low-latitude Pi2 pulsations are associated with a plasmaspheric process, not periodic BBFs, considering that the plasmapause is typically located at $4 < L_m < 6$. In the direct BBF-driven model, the amplitude of the compressional oscillation outside the plasmasphere decreases as the distance from the source region increases. A recent numerical study (Lysak et al., 2015) showing the response of the dipole magnetosphere to a compressional pulse presents the wave features of Pi2 pulsations at $L < 10$ generated by a compressional pulse, which simulates the impinging of a fast flow on the inner magnetosphere. The study shows that coherent waves structure is established in the plasmasphere by the pulse, which indicates that periodic compressional pulses driven by BBFs in the magnetotail generate PC/PVR mode in the plasmasphere. They also showed Pi2 pulsations waveforms in the compressional component from $L \sim 2$ to $L \sim 10$. The amplitudes of compressional Pi2 waves decreased earthward from the $L \sim 10$ to the plasmapause while it was enhanced in the plasmasphere because of the plasmaspheric eigenmode. This result indicates that the L dependence of Pi2 amplitude derived by BBF has the same tendency as our results, in which the B_P-H amplitude ratio has a peak at the plasmapause. In addition, the Mlat dependence of the B_R-H and B_P-H power ratios shown in Figure 8 indicates the equatorial nodal structure of these waves. The direct BBF-driven mode may also cause such Mlat dependence in the inner magnetosphere. To interpret the spatial distribution of the B-H power ratio more accurately, we may need to consider variation in the geometry of the background magnetic field lines, ionospheric condition, and the plasma density in each L shell. These variations may affect the B-H power ratio of Pi2 pulsations in the inner magnetosphere. For instance using analytical and numerical solutions to the guided poloidal Alfven wave equations in a dipole field, Ozeke and Mann (2004) reported that the field-aligned distributions of the magnetic field amplitudes for the half- or quarter-wavelength mode are altered as the ionospheric conductivities become increasingly asymmetric. Although the Pi2 pulsations are global mode waves, the local variations in the geometry of the background magnetic field line, plasma density, and the ionospheric conductivities may cause the field-aligned magnetic field distributions of the Pi2 pulsations to change; these local variations in each L shell may alter the global distribution of the Pi2 pulsation amplitudes. Therefore, using only the power ratio profile shown in Figures 8 and 10b, we cannot distinguish whether the Pi2 pulsations observed by Arase are excited by the BBF or PVR mode. However, the ΔL profile of the B_P-H cross phase cannot be explained by the direct BBF-driven model. Owing to compressional waves propagating in the inner magnetosphere, the phase distribution of the Pi2 pulsations outside the plasmasphere would change linearly (Lysak et al., 2015). This would mean that the phase of the compressional waves in the inner magnetosphere would shift gradually from the source region to the plasmapause. As shown in Figure 10d, the B_P-H cross phase outside the plasmasphere is almost constant (∼180°) and does not show a linear change, which is inconsistent with the direct BBF-driven model.

To clarify the generation mechanism of low-latitude Pi2 pulsations in more detail, statistical studies using multiple-satellite observations, in which Pi2 pulsations in the inner magnetosphere ($L < 6$) are compared to Pi2 pulsations in the higher L region and plasma flows oscillations in the tail, are needed. Wang et al. (2020) statistically assessed the midnight conjunction events of Pi2 pulsations at geosynchronous distances and in the plasma sheet and BBFs, using observations from the THEMIS and Geostationary Operational Environmental Satellites (GOES). They compared the enhancement of the 6–25 mHz bandpassed compressional magnetic perturbations of the GOES data to the enhancement of the 6–25 mHz bandpassed compressional magnetic perturbations and flow speeds of the THEMIS data. They suggested that all Pi2 enhancements were associated with BBFs. However, to confirm that periodic BBFs in the magnetotail directly drive Pi2 pulsations in the inner magnetosphere, one should compare the waveforms of periodic plasma flows in the plasma sheet and the magnetic perturbations in the inner magnetosphere. An event study by Takahashi et al. (2018) showed that periodic plasma flows with a period of 2 min in the magnetotail were observed by the THEMIS satellite when compressional Pi2 pulsations were detected in the plasmasphere by the Van Allen Probes. The coherence between the periodicity of the plasma flow and compressional Pi2 pulsations was low. This result suggests that Pi2 pulsations in the inner magnetosphere are generated by a broadband energy source, although the plasma flows in the magnetosphere show periodicity with the Pi2 band frequency. Statistical cross-spectral analysis of the flow oscillation in the magnetotail and Pi2 pulsations in the inner magnetosphere ($L < 6$) is needed to reveal whether the periodic plasma flows play the role of a pulse-by-pulse driver or a broadband energy driver to the Pi2 pulsations in the inner magnetosphere.

5. Summary and Conclusions

We statistically investigated the spatial properties of Pi2 pulsations in the inner magnetosphere, which have high coherence with Pi2 pulsations at low-latitude ground stations, in relation to the plasmapause, using magnetic field data from the Arase satellite for the period from March 2017 to September 2019. In the approximately 2.5 years of observations, the Arase orbit covered wide latitudinal (|Mlat| < 45°) and longitudinal ranges. The number of high-coherence events relative to Pi2 pulsations at the low-latitude ground stations is largest in the compressional component. The MLT distribution of the high-coherence B_P event occurrence probability and the B_P-H power ratio show that the source regions at low- and mid-latitudes are located on the nightside. For the nightside high-coherence poloidal events, we identified the L_{pp} and defined the distance from the plasmapause as $\Delta L = L_{\mathrm{m}} - L_{\mathrm{pp}}$, using electron density data from Arase. We investigated the ΔL dependence of the B–H power ratio and cross phase for high-coherence poloidal events. The B_R-H power ratio was almost constant near the plasmapause. The B_R-H cross phase was distributed at ~0° and ~180° in the northern and southern hemispheres, respectively. The B_P-H power ratio likely had a gradual peak at ΔL ~0. The B_P-H cross phase clearly changed from 0° to 180° in the vicinity of the plasmapause (ΔL ~0) and remained at ~180° outside the plasmapause ($\Delta L > 0$). The ΔL distribution also show that off-equatorial B_P high-coherence events at |Mlat| > 15° exist beyond the plasmasphere with the large distance from the plasmapause ($\Delta L > 1$) while high-coherence B_R events are confined to the vicinity of the plasmapause ($\Delta L < 1$). Although Pi2 pulsations were excited further away from the magnetic equator (|Mlat| > 15°) as well as close to it, the power ratio, and cross-phase properties relative to the plasmapause are consistent with the PVR mode across a wide latitudinal range.

Data Availability Statement

Data from the ERG (Arase) satellite were obtained from the ERG Science Center operated by ISAS/JAXA and ISEE/Nagoya University (https://ergsc.isee.nagoya-u.ac.jp/index.shtml.en, Miyoshi, Hori, et al., 2018). The present study analyzed MGF-L2 v03_04 data (Matsuoka, Teramoto, Imajo, et al., 2018), PWE/HFA-L3 v01_02 data (Kasahara et al., 2021), and Orbit L2 v02 (Miyoshi et al., 2018a) and L3 v01 (Miyoshi et al., 2018b) data. The geomagnetic field data from Honolulu, San Juan, and Guam were provided by the U.S. Geological Survey stations (https://www.usgs.gov/natural-hazards/geomagnetism and http://themis.ssl.berkeley.edu/data/themis/thg/l2/mag/). The Wp index is available at https://doi.org/10.17593/13437-46800. Data access and processing were performed using SPEDAS V4.1 (see Angelopoulos et al., 2019).

Acknowledgments

We acknowledge the Helmholtz Center Potsdam-GFZ German Research Center for Geosciences for providing the Kp index (https://www.gfz-potsdam.de/en/home/). This study is supported by the Japan Society for the Promotion of Science (JSPS), Grant-in-Aid for Scientific Research (C) (19K03948). Y. M. is supported by the JSPS Grant-in-Aid for Scientific Research (16H06286, 17H00728, 20H01959) S. I. is supported by the JSPS, Grant-in-Aid for Young Scientists (21K13977). I. S. is supported by the JSPS, Grant-in-Aid for Scientific Research (17H06140).

References

Angelopoulos, V., Baumjohann, W., Kennel, C. F., Coroniti, F. V., Kivelson, M. G., Pellat, R., et al. (1992). Bursty bulk flows in the inner central plasma sheet. *Journal of Geophysical Research*, *97*(A4), 4027–4039. https://doi.org/10.1029/91JA02701

Angelopoulos, V., Cruce, P., Drozdov, A., Grimes, E. W., Hatzigeorgiu, N., King, D. A., et al. (2019). The space physics environment data analysis system (SPEDAS). *Space Science Reviews*, *215*(1), 9. https://doi.org/10.1007/s11214-018-0576-4

Collier, A. B., Hughes, A. R. W., Blomberg, L. G., & Sutcliffe, P. R. (2006). Evidence of standing waves during a Pi2 pulsation event observed on Cluster. *Annales Geophysicae*, *24*(10), 2719–2733. https://doi.org/10.5194/angeo-24-2719-2006

Gabrielse, C., Angelopoulos, V., Runov, A., & Turner, D. L. (2014). Statistical characteristics of particle injections throughout the equatorial magnetotail. *Journal of Geophysical Research: Space Physics*, *119*(4), 2512–2535. https://doi.org/10.1002/2013JA019638

Ghamry, E., Kim, K.-H., Kwon, H.-J., Lee, D.-H., Park, J. S., Choi, J., et al. (2015). Simultaneous Pi2 observations by the van allen probes inside and outside the plasmasphere. *Journal of Geophysical Research: Space Physics*, *120*(6), 4567–4575. https://doi.org/10.1002/2015JA021095

Jacobs, J. A. (1970). *Geomagnetic Micropulsations*, Springer. https://doi.org/10.1007/978-3-642-86828-3

Kasahara, Y., Kasaba, Y., Kojima, H., Yagitani, S., Ishisaka, K., Kumamoto, A., et al. (2018). The plasma wave experiment (PWE) on board the Arase (ERG) satellite. *Earth Planets and Space*, *70*(1), 86. https://doi.org/10.1186/s40623-018-0842-4

Kasahara, Y., A. Kumamoto, F. Tsuchiya, H. Kojima, S. Matsuda, A. Matsuoka, et al. (2021). *The PWE/HFA instrument Level-3 electron density data of Exploration of energization and Radiation in Geospace (ERG) Arase satellite, version 01_02*. ERG Science Center, Institute for Space-Earth Environmental Research, Nagoya University. https://doi.org/10.34515/DATA.ERG-10001z

Keiling, A., & Takahashi, K. (2011). Review of Pi2 Models. *Space Science Reviews*, *161*(1), 63–148. https://doi.org/10.1007/s11214-011-9818-4

Keiling, A., Wygant, J. R., Cattell, C., Kim, K.-H., Russell, C. T., Milling, D. K., et al. (2001). Pi2 pulsations observed with the Polar satellite and ground stations: Coupling of trapped and propagating fast mode waves to a midlatitude field line resonance. *Journal of Geophysical Research: Space Physics*, *106*(A11), 25891–25904. https://doi.org/10.1029/2001JA900082

Kepko, L., & Kivelson, M. (1999). Generation of Pi2 pulsations by bursty bulk flows. *Journal of Geophysical Research: Space Physics*, *104*(A11), 25021–25034. http://doi.org/10.1029/1999ja900361

Kepko, L., Kivelson, M. G., & Yumoto, K. (2001). Flow bursts, braking, and Pi2 pulsations. *Journal of Geophysical Research: Space Physics*, *106*(A2), 1903–1915. http://doi.org/10.1029/2000ja000158

Kim, K.-H., Lee, D.-H., Takahashi, K., Russell, C. T., Moon, Y.-J., & Yumoto, K. (2005). Pi2 pulsations observed from the Polar satellite outside the plasmapause. *Geophysical Research Letters*, *32*, L18102. https://doi.org/10.1029/2005GL023872

Kumamoto, A., Tsuchiya, F., Kasahara, Y., Kasaba, Y., Kojima, H., Yagitani, S., et al. (2018). High frequency analyzer (HFA) of plasma wave Experiment (PWE) onboard the Arase spacecraft. *Earth Planets and Space*, *70*(1), 82. https://doi.org/10.1186/s40623-018-0854-0

Kwon, H.-J., Kim, K.-H., Jun, C.-W., Takahashi, K., Lee, D.-H., Lee, E., et al. (2013). Low-latitude Pi2 pulsations during intervals of quiet geomagnetic conditions (Kp≤1). *Journal of Geophysical Research: Space Physics*. *118*(10), 6145–6153. https://doi.org/10.1002/jgra.50582

Lee, D.-H. (1996). Dynamics of MHD wave propagation in the low-latitude magnetosphere. *Journal of Geophysical Research: Space Physics*, *101*(A7), 15371–15386. https://doi.org/10.1029/96JA00608

Lee, D.-H., & Takahashi, K. (2006). MHD eigenmodes in the inner magnetosphere. In *Magnetospheric ULF Waves: Synthesis and New Directions* (Vol. 169, pp. 73). https://doi.org/10.1029/169GM07

Lin, C. A., Lee, L. C., & Sun, Y. J. (1991). Observations of Pi 2 pulsations at a very low latitude (L = 1.06) station and magnetospheric cavity resonances, *Journal of Geophysical Research: Space Physics*, *96*(A12), 21105–21113, https://doi.org/10.1029/91JA02029

Liu, J., Angelopoulos, V., Runov, A., & Zhou, X.-Z. (2013). On the current sheets surrounding dipolarizing flux bundles in the magnetotail: The case for wedgelets. *Journal of Geophysical Research: Space Physics*, *118*(5), 2000–2020. https://doi.org/10.1002/jgra.50092

Luo, H., Chen, G. X., Du, A. M., Angelopoulos, V., Xu, W. Y., Zhao, X. D., et al. (2011). THEMIS multipoint observations of Pi2 pulsations inside and outside the plasmasphere. *Journal of Geophysical Research: Space Physics, 116*, A12206. https://doi.org/10.1029/2011JA016746

Lysak, R. L., Song, Y., Sciffer, M. D., & Waters, C. L. (2015). Propagation of Pi2 pulsations in a dipole model of the magnetosphere. *Journal of Geophysical Research: Space Physics*, *120*(1), 355–367. https://doi.org/10.1002/2014JA020625

Matsuoka, A., Teramoto, M., Imajo, S., Kurita, S., Miyoshi, Y., & Shinohara, I. (2018). *The MGF instrument level-2 spin-averaged magnetic field data of exploration of energization and radiation in geospace (ERG) Arase satellite, version 03_04*. ERG Science Center, Institute for Space-Earth Environmental Research, Nagoya University. https://doi.org/10.34515/DATA.ERG-06001

Matsuoka, A., Teramoto, M., Nomura, R., Nosé, M., Fujimoto, A., Tanaka, Y., et al. (2018). The ARASE (ERG) magnetic field investigation. *Earth Planets and Space*, *70*(1), 43. https://doi.org/10.1186/s40623-018-0800-1

McPherron, R. L., Hsu, T.-S., Kissinger, J., Chu, X., & Angelopoulos, V. (2011). Characteristics of plasma flows at the inner edge of the plasma sheet. *Journal of Geophysical Research: Space Physics*, *116*(A5). https://doi.org/10.1029/2010ja015923

Miyoshi, Y., Hori, T., Shoji, M., Teramoto, M., Chang, T. F., Segawa, T., et al. (2018). The ERG science center. *Earth Planets and Space*, *70*(1), 96. https://doi.org/10.1186/s40623-018-0867-8

Miyoshi, Y., Shinohara, I., & Jun, C.-W. (2018a). *The level-2 orbit data of exploration of energization and radiation in geospace (ERG) Arase satellite*, version 03. Institute for Space-Earth Environmental Research, Nagoya University. https://doi.org/10.34515/DATA.ERG-12000

Miyoshi, Y., Shinohara, I. & Jun, C.-W. (2018b). *The level-3 orbit data of exploration of energization and radiation in geospace (ERG) Arase satellite*, version 01. Institute for Space-Earth Environmental Research, Nagoya University. https://doi.org/10.34515/DATA.ERG-12001

Miyoshi, Y., Shinohara, I., Takashima, T., Asamura, K., Higashio, N., Mitani, T., et al. (2018). Geospace exploration project ERG. *Earth Planets and Space*, *70*(1), 101. https://doi.org/10.1186/s40623-018-0862-0

Nosé, M. (1999). Automated detection of Pi 2 pulsations using wavelet analysis: 2. An application for dayside Pi 2 pulsation study. *Earth Planets and Space*, *51*, 23–32, https://doi.org/10.1186/BF03352206

Nosé, M., Iyemori, T., Wang, L., Hitchman, A., Matzka, J., Feller, M. et al. (2012). Wp index: A new substorm index derived from high-resolution geomagnetic field data at low latitude. *Space Weather*, *10*(8). http://doi.org/10.1029/2012sw000785

Nosé, M., Matsuoka, A., Kumamoto, A., Kasahara, Y., Goldstein, J., Teramoto, M., et al. (2018). Longitudinal structure of oxygen torus in the inner magnetosphere: Simultaneous observations by Arase and Van Allen Probe A. *Geophysical Research Letters*, *45*, 10177–10184. https://doi.org/10.1029/2018GL080122

Nosé, M., Matsuoka, A., Kumamoto, A., Kasahara, Y., Teramoto, M., Kurita, S., et al. (2020). Oxygen torus and its coincidence with EMIC wave in the deep inner magnetosphere: Van Allen Probe B and Arase observations. *Earth Planets and Space*, *72*(1), 111. https://doi.org/10.1186/s40623-020-01235-w

Osaki, H., Takahashi, K., Fukunishi, H., Nagatsuma, T., Oya, H., Matsuoka, A., & Milling, D. K. (1998). Pi2 pulsations observed from the Akebono satellite in the plasmasphere. *Journal of Geophysical Research: Space Physics*, *103*(A8), 17605–17615. https://doi.org/10.1029/97ja03012

Ozeke, L. G., & Mann, I. R. (2004). Modeling the properties of guided poloidal Alfvén waves with finite asymmetric ionospheric conductivities in a dipole field. *Journal of Geophysical Research*, *109*(A5). https://doi.org/10.1029/2003ja010151

Rostoker, G., Akasofu, S.-I., Foster, J., Greenwald, R., Kamide, Y., Kawasaki, K., et al. (1980). Magnetospheric substorms—Definition and signatures. *Journal of Geophysical Research, 85*(A4), 1663–1668. https://doi.org/10.1029/JA085iA04p01663

Runov, A., Sergeev, V. A., Baumjohann, W., Nakamura, R., Apatenkov, S., Asano, Y., et al. (2005). Electric current and magnetic field geometry in flapping magnetotail current sheets. *Annales Geophysicae*, *23*(4), 1391–1403. https://doi.org/10.5194/angeo-23-1391-2005

Saito, T., & Matsushita, S. (1968). Solar cycle effects on geomagnetic Pi 2 pulsations. *Journal of Geophysical Research*, *73*(1), 267–286. https://doi.org/10.1029/JA073i001p00267

Sergeev, V. A., Chernyaev, I. A., Dubyagin, S. V., Miyashita, Y., Angelopoulos, V., Boakes, P. D., et al. (2012). Energetic particle injections to geostationary orbit: Relationship to flow bursts and magnetospheric state. *Journal of Geophysical Research*, *117*, A10207. https://doi.org/10.1029/2012JA017773

Takahashi, K., Anderson, R. R., & Hughes, W. J. (2003). Pi2 pulsations with second harmonic: CRRES observations in the plasmasphere. *Journal of Geophysical Research, 108*, 1242. https://doi.org/10.1029/2003JA009847

Takahashi, K., Hartinger, M. D., Vellante, M., Heilig, B., Lysak, R. L., Lee, D.-H., et al. (2018). Roles of flow braking, plasmaspheric virtual resonances, and ionospheric currents in producing ground Pi2 pulsations. *Journal of Geophysical Research: Space Physics*, *123*(11), 9187–9203. https://doi.org/10.1029/2018JA025664

Takahashi, K., Lee, D. H., Nosé, M., Anderson, R. R., & Hughes, W. J. (2003). CRRES electric field study of the radial mode structure of Pi2 pulsations. *Journal of Geophysical Research: Space Physics*, *108*(A5), 1210. https://doi.org/10.1029/2002JA009761

Takahashi, K., & Liou, K. (2004). Longitudinal structure of low-latitude Pi2 pulsations and its dependence on aurora. *Journal of Geophysical Research*, *109*, A12206. https://doi.org/10.1029/2004JA010580

Takahashi, K., Ohtani, S., & Anderson, B. J. (1995). Statistical analysis of Pi 2 pulsations observed by the AMPTE CCE Spacecraft in the inner magnetosphere. *Journal of Geophysical Research*, *100*(A11), 21929–21941. https://doi.org/10.1029/95JA01849

Takahashi, K., Ohtani, S., Denton, R. E., Hughes, W. J., & Anderson, R. R. (2008). Ion composition in the plasma trough and plasma plume derived from a Combined Release and Radiation Effects Satellite magnetoseismic study. *Journal of Geophysical Research*, *113*, A12203. https://doi.org/10.1029/2008JA013248

Teramoto, M., Nosé, M., & Sutcliffe, P. R. (2008). Statistical analysis of Pi2 pulsations inside and outside the plasmasphere observed by the polar orbiting DE-1 satellite. *Journal of Geophysical Research: Space Physics*, *113*, A07203. https://doi.org/10.1029/2007JA012740

Teramoto, M., Takahashi, K., Nosé, M., Lee, D.-H., & Sutcliffe, P. R. (2011). Pi2 pulsations in the inner magnetosphere simultaneously observed by the active magnetospheric particle tracer explorers/charge composition explorer and dynamics explorer 1 satellites. *Journal of Geophysical Research: Space Physics*, *116*, A07225. https://doi.org/10.1029/2010JA016199

Tsyganenko, N. A., & Sitnov, M. I. (2005). Modeling the dynamics of the inner magnetosphere during strong geomagnetic storms. *Journal of Geophysical Research*, *110*(A3). https://doi.org/10.1029/2004ja010798

Wang, C.-P., Xing, X., Bortnik, J., & Chu, X. (2020). Inward propagation of flow-generated Pi2 waves from the plasma sheet to the inner magnetosphere. *Journal of Geophysical Research: Space Physics*. *125*, e2019JA027581. https://doi.org/10.1029/2019JA027581

World Data Center for Geomagnetism, Kyoto, & Nosé, M. (2016). *Geomagnetic Wp index*. https://doi.org/10.17593/13437-46800